

Structural identification of a bacterial quorum-sensing signal containing boron

Xin Chen*, Stephan Schauder*, Noelle Potier†, Alain Van Dorsselaer†, István Pelczér‡, Bonnie L. Bassler* & Frederick M. Hughson*

* Department of Molecular Biology; and ‡ Department of Chemistry, Princeton University, Princeton, New Jersey 08544-1014, USA

† Laboratoire de Spectrométrie de Masse Bio-Organique, Ecole de Chimie, Polymères et Matériaux, 25 Rue Becquerel, 67087 Strasbourg, France

Cell-cell communication in bacteria is accomplished through the exchange of extracellular signalling molecules called autoinducers. This process, termed quorum sensing, allows bacterial populations to coordinate gene expression. Community cooperation probably enhances the effectiveness of processes such as bioluminescence, virulence factor expression, antibiotic production and biofilm development¹⁻⁴. Unlike other autoinducers, which are specific to a particular species of bacteria, a recently

discovered autoinducer (AI-2)⁵ is produced by a large number of bacterial species. AI-2 has been proposed to serve as a 'universal' signal for inter-species communication^{1,2,6,7}. The chemical identity of AI-2 has, however, proved elusive. Here we present the crystal structure of an AI-2 sensor protein, LuxP, in a complex with autoinducer. The bound ligand is a furanosyl borate diester that bears no resemblance to previously characterized autoinducers. Our findings suggest that addition of naturally occurring borate to an AI-2 precursor generates active AI-2. Furthermore, they indicate a potential biological role for boron, an element required by a number of organisms but for unknown reasons.

AI-2 was originally identified in the bioluminescent marine bacterium *Vibrio harveyi* as one of two autoinducers that regulate light production in response to cell density^{5,8}. The synthase required for AI-2 production, LuxS, is widely conserved among Gram-negative and Gram-positive bacteria⁷. AI-2 is produced from *S*-adenosylmethionine in at least three enzymatic steps (Fig. 1a). Consumption of *S*-adenosylmethionine as a methyl donor produces *S*-adenosylhomocysteine, which is subsequently hydrolysed by the nucleosidase Pfs to yield adenine and *S*-ribosylhomocysteine^{9,10}. Subsequently, *S*-ribosylhomocysteine is converted to 4,5-dihydroxy-2,3-pentanedione (DPD) and homocysteine^{11,12}. This reaction is catalysed by LuxS^{13,14}. DPD probably forms a cyclic molecule,

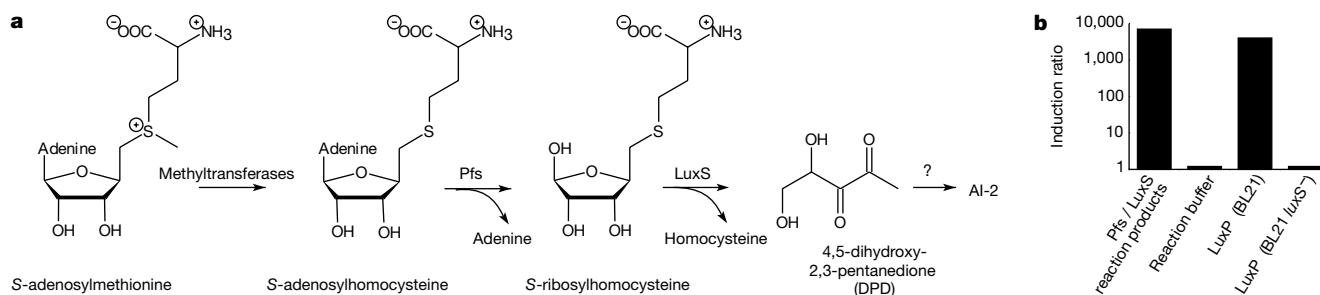


Figure 1 The autoinducer AI-2, synthesized by LuxS, is bound by the sensor protein LuxP. **a**, Biosynthesis of the AI-2 precursor 4,5-dihydroxy-2,3-pentanedione (DPD) from *S*-adenosylmethionine⁹⁻¹³. **b**, Induction of bioluminescence in the *V. harveyi* bioassay¹³ was measured following the addition of the products of an *in vitro* reaction of

S-adenosylhomocysteine with Pfs and LuxS proteins¹³, reaction buffer, or AI-2 released from LuxP overproduced in LuxS⁺ or LuxS⁻ *E. coli* BL21. Concentrations of AI-2 in the Pfs/LuxS and LuxP (BL21) reactions were estimated to be 20 μM (see Methods).

Table 1 Phasing and refinement statistics

	Native	KPtCl ₄	K ₃ UO ₃ F ₅	Sm(NO ₃) ₃	Eu(NO ₃) ₃
Resolution (Å)	1.5	2.2	2.5	2.4	2.8
Unique reflections	61,620	17,815	13,657	13,483	9,824
Redundancy	5.5	6	3.2	3.6	3.2
R _{sym} (%)	3.5 (25)	6.3 (32)	9.4 (33)	7.8 (25)	8.5 (29)
Complete (%)	100	100	99.7	99.6	93.1
MIR phasing at 2.8 Å					
Heavy atom sites		3	3	3	2
Phasing power acentric/centric		0.69/0.66	1.35/1.13	0.48/0.42	1.2/0.81
R _{critis} acentric/centric		0.87/0.85	0.78/0.76	0.95/0.90	0.80/0.82
Anomalous R _{critis}		0.91	0.78	0.93	n/a
Combined figure of merit MLPHARE/DM ²⁵		0.60/0.82			
Refinement					
Resolution (Å)	25-1.5				
Reflections (>σ)	53,816				
R _{cryst}	0.214 (0.274)				
R _{free}	0.239 (0.317)				
Root-mean-square (r.m.s) deviation					
Bond length	0.007 Å				
Bond angle	1.3°				
Average B factor					
Protein	24.1				
AI-2	11.7				
Water molecules	34.1				
All atoms	25.3				

Data in parentheses are for the highest-resolution shell. $R_{sym} = \sum_i \sum_h |I_i(h) - \langle I(h) \rangle| / \sum_i \sum_h I_i(h)$, where $I_i(h)$ is the *i*th measurement of $I(h)$ for reflection h . Phasing power is $\langle |F_{ph}| \rangle / E$, where $\langle |F_{ph}| \rangle$ is the r.m.s. structure factor amplitude for anomalous scatterers and E is the estimated lack-of-closure error. $R_{critis} = \sum |F_p \pm F_{ph}| - F_c / \sum |F_p \pm F_{ph}|$. $R_{cryst} = \sum |F_o| - |F_c| / \sum |F_o|$, calculated with a working set of reflections. R_{free} is R_{cryst} calculated with only the test set of reflections, comprising a randomly selected 8% of the data, not used during refinement.

and possibly undergoes further rearrangements, to yield AI-2 (ref. 13).

The detection of AI-2 by *V. harveyi* requires two proteins, LuxP and LuxQ⁸. LuxP belongs to a large family of periplasmic binding proteins whose members bind diverse ligands¹⁵, while LuxQ is a two-component hybrid sensor kinase embedded in the bacterial inner membrane⁸. Several lines of evidence suggest that LuxP is the primary AI-2 receptor. First, LuxP is homologous to the periplasmic ribose-binding proteins of *Escherichia coli* and *Salmonella typhimurium*⁸. This homology is of particular interest as AI-2 is derived from a ribosyl moiety (Fig. 1a). Second, AI-2 is the ligand for a LuxP homologue (LsrB) in *S. typhimurium*¹⁶. Third, purified recombinant LuxP, overproduced in the LuxS⁺ *E. coli* strain BL21,

releases substantial AI-2 signalling activity upon thermal denaturation (Fig. 1b). This activity is nearly equivalent to that produced in an *in vitro* reaction in which *S*-adenosylhomocysteine is incubated with purified recombinant Pfs and LuxS¹³ (Fig. 1b). LuxP overproduced in a LuxS⁻ BL21 strain releases no AI-2 activity upon denaturation. These results demonstrate that LuxP binds AI-2. Furthermore, binding is tight, because the AI-2 remains associated during chromatographic purification. In quorum sensing, the periplasmic LuxP-AI-2 complex probably interacts with LuxQ to transduce the autoinducer signal.

The X-ray crystal structure of recombinant *V. harveyi* LuxP, overproduced in the LuxS⁺ *E. coli* strain BL21, was determined by multiple isomorphous replacement at (MIR) at 2.8 Å resolution and

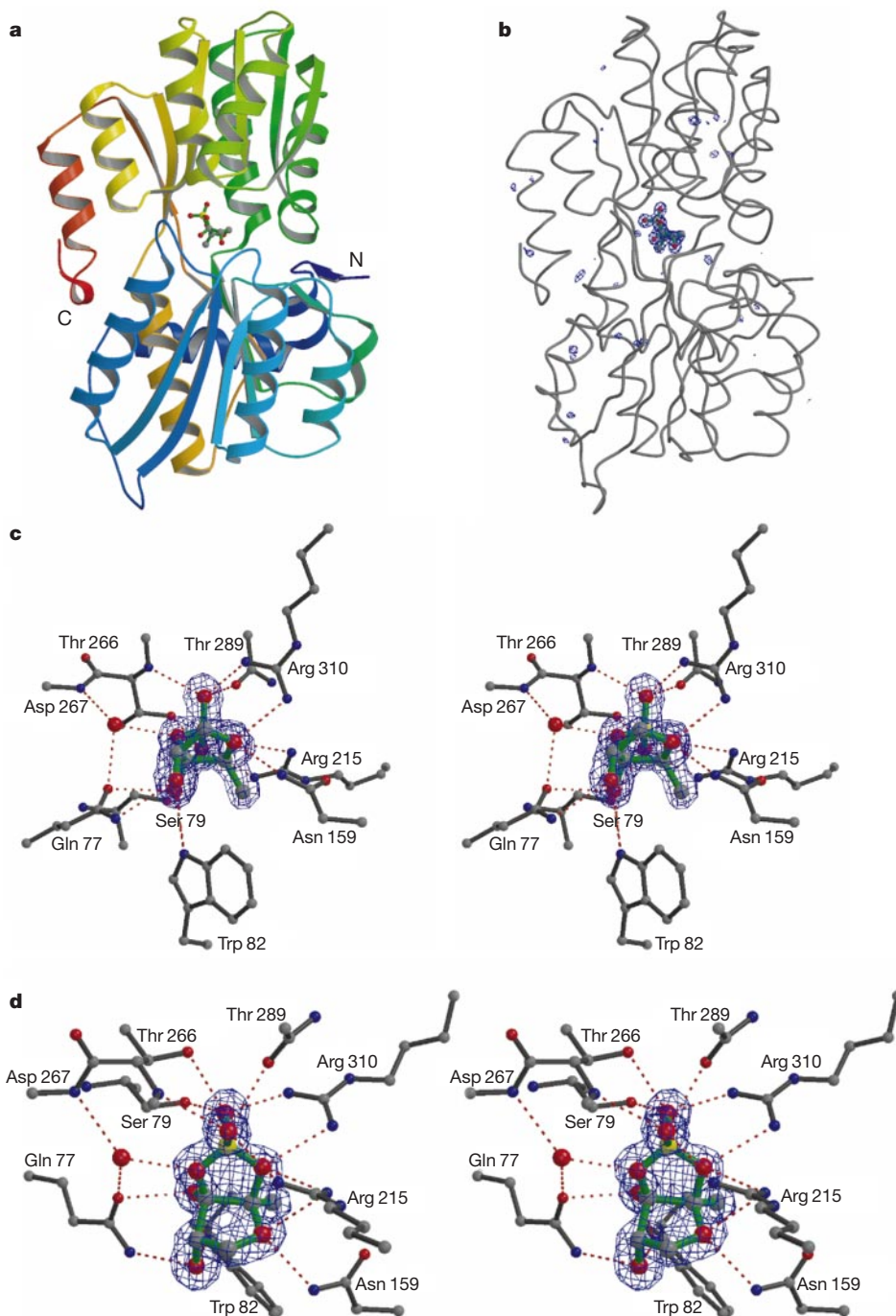


Figure 2 Structure of LuxP-AI-2 complex. **a**, Overview. **b-d**, $F_o - F_c$ difference electron density (contoured at 4σ) calculated using phases derived from the model before AI-2 addition. The final refined model for AI-2 is shown superimposed on this density. Boron,

oxygen, nitrogen and carbon are coloured yellow, red, blue and grey, respectively. In the stereoviews shown in **c-d**, hydrogen bonds are shown as dashed red lines. Figure prepared using O²⁶, Molscript²⁸/Bobscrip²⁹ and Raster 3D³⁰.

refined to 1.5 Å resolution (Table 1). Like other periplasmic binding proteins¹⁵, LuxP consists of two similar domains connected by a three-stranded hinge (Fig. 2a). The deep cleft between the two LuxP domains contains additional electron density, corresponding to the AI-2 ligand, that was clearly visible even in initial experimental electron density maps at 2.8 Å resolution. The location of this density is clearly analogous to that of ligands in other periplasmic

binding proteins. The quality of the additional electron density improved steadily as refinement of the protein model progressed until, at 1.5 Å resolution, it was straightforward to construct a model for AI-2 by positioning atoms in the difference electron density (Fig. 2b–d).

Because it is derived from the ribose moiety of S-ribosylhomocysteine, AI-2 was initially modelled as a carbohydrate. The assignment of atom type at each position was dictated by both the valence and the local chemical environment within the protein. Thus, tetrahedrally substituted atoms were deemed to be carbons, whereas atoms within hydrogen-bonding distance of at least one (but generally two to three) polar protein atoms or buried water molecules were deemed to be oxygens. Weak bond length and bond angle restraints were applied to the ligand during subsequent refinement. The resulting structural model for the LuxP-AI-2 complex has an R_{cryst} and R_{free} of 0.21 and 0.24, respectively, and exhibits excellent geometry (Table 1). No orientational or chemical heterogeneity of the buried ligand is evident in the crystallographic electron density.

The proposed AI-2 structure contains two fused five-membered rings stabilized within the LuxP binding site by numerous polar interactions (Fig. 3a). Several candidates were considered for the atom bridging the diester. We suggest that it is boron, on the basis of several considerations. Although boron and carbon are not reliably distinguishable on the basis of electron density at this resolution, the presence of carbon at this position would result in a highly unstable orthocarbonate moiety, whereas the borate diester is relatively stable¹⁷. Heavier atoms, such as phosphorus or sulphur, could bridge the diester instead of boron. This possibility can, however, be eliminated because these atoms would give rise to markedly stronger electron density than is observed. In fact, the electron density at this position, although clear, is the weakest of the eight positions in the fused ring structure, consistent with its assignment as boron.

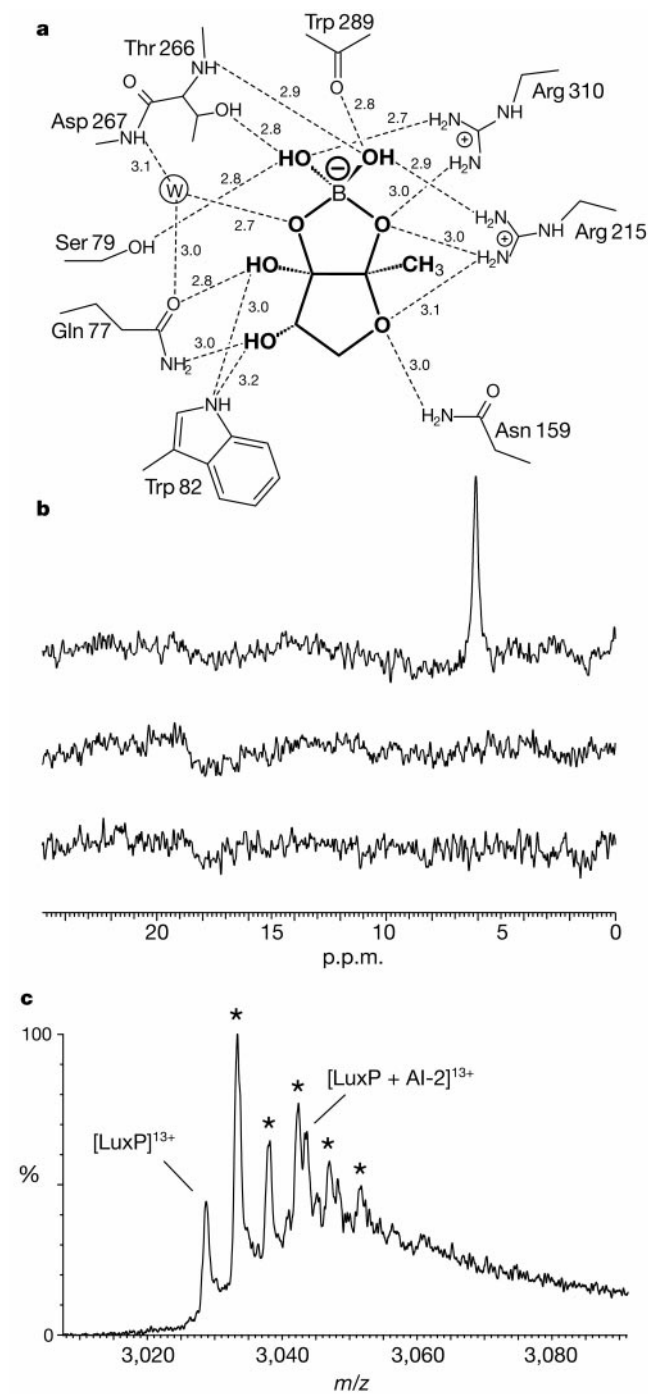


Figure 3 Structure of AI-2. **a**, AI-2 and the hydrogen bond network that stabilizes it in the LuxP binding site. O–O or O–N distances for potential hydrogen bonds are shown in ångströms. **b**, ¹¹B NMR spectra of LuxP overproduced in *E. coli* BL21 (top trace) or BL21 *luxS*[−] (bottom trace). The spectrum of the ultrafiltrate from the BL21 sample is also shown (middle trace). **c**, Mass spectrometric analysis of LuxP-AI-2 in 200 mM ammonium acetate buffer. LuxP alone (39,295.6 ± 1.2), a number of acetate adducts (in increments of 60 daltons; marked with asterisks), and LuxP-AI-2 (39,489.8 ± 2.7) peaks are observed. Approximately 15% of the LuxP retains AI-2. Only acetate adducts are observed in an identical experiment with apo-LuxP (not shown).

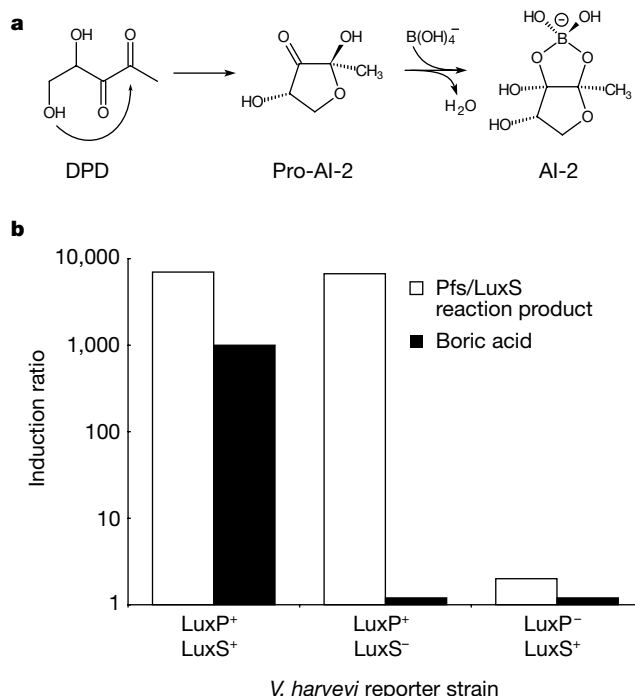


Figure 4 Synthesis of AI-2 from DPD and borate. **a**, Cyclization is thermodynamically favourable. The position of the equilibrium in the second step will depend on the concentrations of pro-AI-2 and borate (B(OH)₄[−]). Other possible reactions are not shown. **b**, Light induction by boric acid. The induction of light production in *V. harveyi* reporter strains relative to a buffer control was measured following the addition of *in vitro* Pfs/LuxS reaction products (approximately 20 μM; white bars) or 1 mM boric acid (black bars). Addition of boric acid does not cause a pH change.

The positively charged side chains of Arg 215 and Arg 310 form hydrogen bonds with three of the four borate oxygens and appear to stabilize the negative charge on the borate (Figs 2c, d and 3a).

To confirm that the ligand contains boron, we carried out ^{11}B NMR spectroscopy. As predicted, the spectrum of the LuxP-AI-2 complex shows a peak signifying the presence of boron (Fig. 3b, top trace). The chemical shift for this peak (6.2 p.p.m.) is within the range (3.9–6.2 p.p.m.) observed for borate esters of carbohydrate 1,2-diols¹⁸. For comparison, borate esters of 1,3-diols and boric acid display chemical shifts of 0.3–0.9 and 18.8 p.p.m. respectively. The ^{11}B NMR peak disappeared after ultrafiltration to remove protein (Fig. 3b, middle trace). Furthermore, it was not observed in apo-LuxP overproduced in LuxS⁻ BL21 *E. coli* (Fig. 3b, bottom trace).

To provide additional support for the AI-2 structure proposed here, we determined the mass of the LuxP-AI-2 complex using electrospray ionization mass spectrometry (ESI-MS). Under optimized conditions, peaks are observed for both LuxP and LuxP-AI-2 at molecular masses that differ by 194.2 ± 3.0 daltons (Fig. 3c). This mass increment agrees closely with the molecular mass of the proposed AI-2 molecule (192.9 daltons). We were unable to recover a species corresponding to AI-2 alone.

A chemically straightforward route connects DPD, the product of the LuxS-catalysed reaction, to AI-2 (Fig. 4a). The cyclic form of DPD, which we name pro-AI-2, can react with borate to form a cyclic borate diester. The boric acid required for this reaction is widely available in the biosphere; for example, the average boric acid concentration in sea water is approximately 0.4 mM (ref. 19). (Borate, with a pK_a of 9.2, is present largely as undissociated boric acid at neutral pH.) Furthermore, furanosyl borate diesters similar in structure to AI-2 are relatively stable²⁰. Surprisingly, furanoid rings expected to form stable borate addition products are rare in nature with only two, ribose and apiose, known to have this configuration in their physiological derivatives²¹. In addition to AI-2, other borate adducts may be produced from cyclic derivatives of DPD. Only AI-2, however, is observed in the LuxP crystal structure determined here. Given the large number of specific hydrogen bonds mediating the LuxP-AI-2 interaction (Fig. 3a), it seems unlikely that alternative products could bind with comparable affinity. Taken together, our results provide strong evidence that AI-2 is a cyclic borate diester derivative of DPD. This compound may provide a fruitful lead in the development of antibacterial drugs that target quorum sensing.

Boric acid has a dramatic effect on AI-2 signalling in *V. harveyi*, as shown using a LuxP⁺, LuxS⁺ reporter strain. This strain produces its own AI-2. Endogenously produced AI-2 stimulates light production, but only after a delay during which the AI-2 concentration builds to a threshold stimulatory level. During this delay period, the addition of the activity produced by the *in vitro* reaction of S-adenosylhomocysteine with Pfs and LuxS induces light production. Addition of 1 mM boric acid also results in substantial induction (Fig. 4b). Boric acid concentrations as low as 10 μM caused significant (tenfold) induction (data not shown). Boric acid has no effect on a LuxS⁻ strain that cannot synthesize DPD, nor on a LuxP⁻ strain that lacks the AI-2 sensor (Fig. 4b). Both of the latter strains show wild-type responses to the other *V. harveyi* autoinducer (AI-1) under these experimental conditions (data not shown). Therefore, the induction of bioluminescence by boric acid is specific for the AI-2 detection system.

We conclude that the availability of borate is limiting under the conditions of the autoinducer bioassay. Additional borate may simply drive the spontaneous production of AI-2 from the available pool of pro-AI-2 (see Fig. 4a). Alternatively, it may provide substrate for an unidentified enzyme that catalyses borate addition. In either case, the strong induction by boric acid in the bioassay is consistent with our proposed chemical structure for AI-2. It will be of particular interest to determine whether borate addition normally occurs immediately after DPD synthesis in the cytoplasm of

the autoinducer-producing cell, extracellularly, or in the periplasm of the recipient cell.

We have shown that AI-2 is a novel furanosyl borate diester. By contrast, previously characterized autoinducers are acyl homoserine lactones, modified oligopeptides or quinolones^{1,2}. One of the most unexpected features of the AI-2 molecule is the presence of a boron atom. Boron has previously been found in a small number of polyketide antibiotics²². It is also known to be essential for vascular plants and several other organisms, including cyanobacteria²¹; however, in no case is its functional role well understood. Our results provide evidence for a biochemically defined function for boron in bacterial quorum sensing.

Whereas acyl homoserine lactone and oligopeptide autoinducers are used for communication within a bacterial species, we have proposed that AI-2 is a universal signalling molecule that facilitates inter-species communication^{1,2}. We have previously shown that LuxS enzymes from a variety of bacteria produce AI-2 activity¹³, presumably through the generation of a common intermediate, pro-AI-2. The results presented here show that the AI-2 sensor in *V. harveyi*, LuxP, binds a borate diester of pro-AI-2. Because the biochemical machinery for synthesizing pro-AI-2 is broadly conserved, and borate is widely available, we speculate that AI-2 is produced and detected by diverse bacterial species. If so, our findings are consistent with the hypothesis that AI-2 is a universal signal.

It remains possible, however, that other pro-AI-2 derivatives are generated and serve as signalling molecules in nature. Alternative derivatives need not necessarily contain boron. Isosteric molecules might also be able to activate signalling via LuxP. Indeed, pro-AI-2 could give rise to diverse signals, their relative abundances dictated by the prevailing environmental conditions and the corresponding availability of reactive species. Integrating inputs from a family of molecules similar in structure to AI-2 could provide bacteria with a rich chemical lexicon with which to communicate.

Note added in proof: A requirement for borate in crosslinking plant cell wall polysaccharides was recently reported³¹. □

Methods

LuxP production

Vibrio harveyi LuxP residues 24–365 (lacking the amino-terminal signal peptide) was overproduced as a glutathione S-transferase (GST) fusion protein. *Escherichia coli* strain BL21, carrying a pGEX4T1-LuxP expression plasmid, was grown in Luria-Bertani medium. Protein expression was induced by the addition of 0.5 mM isopropyl β -D-thiogalactopyranoside. The GST fusion protein was purified by glutathione agarose affinity chromatography. After thrombin cleavage, LuxP contained three additional residues at its N terminus (Gly-Ser-Met). The cleaved product was purified by anion exchange chromatography (MonoQ; Pharmacia). LuxP lacking bound AI-2 was overproduced in a LuxS⁻ derivative of BL21 and purified using the same protocol.

Crystallization and diffraction data collection

LuxP (8 mg ml⁻¹) crystallized in 0.1 M Tris-HCl, pH 8.5, 15% PEG 4000, 18% glycerol (v/v) in space group $P2_1$. Native crystals ($a = 42.3 \text{ \AA}$, $b = 77.5 \text{ \AA}$, $c = 52.0 \text{ \AA}$ and $\beta = 96^\circ$) diffracted to 1.5 \AA resolution after flash-freezing at 100 K at NSLS beamline X12C. Derivatives (Table 1) were prepared by soaking crystals for 12–18 h in well buffer containing heavy atoms at 10 mM concentration. Derivative diffraction data at 100 K were collected using an R-AXIS-IV imaging plate detector mounted on a Rigaku 200HB generator. All data were processed using the HKL program package²³.

Structure determination and refinement

Heavy atom positions were located using SOLVE²⁴ and refined using MLPHARE²⁵. Initial phases calculated with MLPHARE were improved by solvent flattening using DM²⁵ (Table 1). An initial protein model was built into the electron density using the program O²⁶ and refined to 1.5 \AA resolution using CNS²⁷. No ligand was included in the model until the R_{cryst} and R_{free} had dropped to 0.24 and 0.26, respectively and 187 water molecules (none of them in the ligand position) had been added to the model. No evidence of disorder or multiple conformations was observed for the protein side chains in the AI-2 binding pocket, making it unlikely that the observed ligand electron density represents a mixture of compounds or binding modes. The present model contains residues 27–364 of LuxP, AI-2 and 273 ordered water molecules, and exhibits excellent geometry, with all residues within the most favoured and additional allowed regions of the Ramachandran plot.

AI-2 bioassay

The *in vitro* Pfs/LuxS reaction was carried out on S-adenosylhomocysteine in 10 mM sodium phosphate, pH 7.5, as described¹³. The resulting yield of AI-2 and/or AI-2 precursors was estimated by measuring the amount of homocysteine released¹³. AI-2 activity was assayed using a *V. harveyi* reporter assay⁶. Reporter strains used were BB170 (LuxP⁺, LuxS⁺)⁵, MM30 (LuxP⁺, LuxS⁻)⁷ and BB886 (LuxP⁺, LuxS⁺)⁸. To release AI-2, LuxP was heated for 10 min at 50 °C, then ultrafiltered to remove denatured protein (BioMax Ultrafree, 5,000 relative molecular mass cutoff). The concentration of AI-2 was estimated by assuming complete recovery.

NMR

¹¹B NMR spectra at 4 °C were collected using a Varian Unity/INOVA spectrometer at 160.5 MHz equipped with a 5-mm tunable X/¹H probe (Nalorac), and were referenced indirectly to BF₃O(Et)₂. 80,000 scans were averaged for each spectrum with a 0.25-s recycle time using an approximately 30° flip-angle pulse. LuxP samples contained 0.2 mM protein in 25 mM HEPES, pH 7.5, 100 mM NaCl. Protein was removed from control samples by ultrafiltration (BioMax Ultrafree, 5,000 relative molecular mass cutoff).

Mass spectrometry

Mass spectrometry was performed using an ESI-TOF mass spectrometer (Q-TOF2, Micromass) on LuxP-AI-2 extensively dialysed against 200 mM ammonium acetate, pH 6.5. To help preserve noncovalent complexes, mild interface conditions were used. Specifically, the declustering voltage (V_c), which controls the kinetic energy of the ions in the interface, was set to 20 V. Data acquired in the positive mode were calibrated using a myoglobin standard.

Received 4 September; accepted 14 November 2001.

1. Miller, M. B. & Bassler, B. L. Quorum sensing in bacteria. *Annu. Rev. Microbiol.* **55**, 165–199 (2001).
2. Schauder, S. & Bassler, B. L. The language of bacteria. *Genes Dev.* **15**, 1468–1480 (2001).
3. de Kievit, T. R. & Iglewski, B. H. Bacterial quorum sensing in pathogenic relationships. *Infect. Immunol.* **68**, 4839–4849 (2000).
4. Kleerebezem, M., Quadri, L. E., Kuipers, O. P. & de Vos, W. M. Quorum sensing by peptide pheromones and two-component signal-transduction systems in Gram-positive bacteria. *Mol. Microbiol.* **24**, 895–904 (1997).
5. Bassler, B. L., Wright, M., Showalter, R. E. & Silverman, M. R. Intercellular signalling in *Vibrio harveyi*: sequence and function of genes regulating expression of luminescence. *Mol. Microbiol.* **9**, 773–786 (1993).
6. Surette, M. G. & Bassler, B. L. Quorum sensing in *Escherichia coli* and *Salmonella typhimurium*. *Proc. Natl Acad. Sci. USA* **95**, 7046–7050 (1998).
7. Surette, M. G., Miller, M. B. & Bassler, B. L. Quorum sensing in *Escherichia coli*, *Salmonella typhimurium*, and *Vibrio harveyi*: a new family of genes responsible for autoinducer production. *Proc. Natl Acad. Sci. USA* **96**, 1639–1644 (1999).
8. Bassler, B. L., Wright, M. & Silverman, M. R. Multiple signalling systems controlling expression of luminescence in *Vibrio harveyi*: sequence and function of genes encoding a second sensory pathway. *Mol. Microbiol.* **13**, 273–286 (1994).
9. Della Ragione, F., Porcelli, M., Carteni-Farina, M., Zappia, V. & Pegg, A. E. *Escherichia coli* S-adenosylhomocysteine/5'-methylthioadenosine nucleosidase. Purification, substrate specificity and mechanism of action. *Biochem. J.* **232**, 335–341 (1985).
10. Cornell, K. A., Swarts, W. E., Barry, R. D. & Riscoe, M. K. Characterization of recombinant *Escherichia coli* 5'-methylthioadenosine/S-adenosylhomocysteine nucleosidase: analysis of enzymatic activity and substrate specificity. *Biochem. Biophys. Res. Commun.* **228**, 724–732 (1996).
11. Miller, C. H. & Duerre, J. A. S-ribosylhomocysteine cleavage enzyme from *Escherichia coli*. *J. Biol. Chem.* **243**, 92–97 (1968).
12. Duerre, J. A. & Walker, R. D. In *The Biochemistry of Adenosylmethionine* (eds Salvatore, F., Borek, E., Zappia, V., Williams-Ashman, H. G. & Schlenk, F.) 43–57 (Columbia Univ. Press, New York, 1977).
13. Schauder, S., Shokat, K., Surette, M. G. & Bassler, B. L. The LuxS family of bacterial autoinducers: biosynthesis of a novel quorum sensing signal molecule. *Mol. Microbiol.* **41**, 463–476 (2001).
14. Lewis, H. A. *et al.* A structural genomics approach to the study of quorum sensing: Crystal structures of three LuxS orthologs. *Structure* **9**, 527–537 (2001).
15. Quioccho, F. A. & Ledvina, P. S. Atomic structure and specificity of bacterial periplasmic receptors for active transport and chemotaxis: variation of common themes. *Mol. Microbiol.* **20**, 17–25 (1996).
16. Taga, M. E., Semmelhack, J. L. & Bassler, B. L. The LuxS-dependent autoinducer AI-2 controls the expression of an ABC transporter that function in AI-2 uptake in *Salmonella typhimurium*. *Mol. Microbiol.* **42**, 777–794 (2001).
17. Böseken, J. The use of boric acid for the determination of the configuration of carbohydrates. *Adv. Carbohydr. Chem.* **4**, 189–210 (1949).
18. van den Berg, R., Peters, J. P. & van Bekkum, H. The structure and (local) stability constants of borate esters of mono- and di-saccharides as studied by ¹¹B and ¹³C NMR spectroscopy. *Carbohydr. Res.* **253**, 1–12 (1994).
19. Bowen, H. J. M. *Trace Elements in Biochemistry* (Academic, London, 1966).
20. Mazurek, M. & Perlin, A. S. Borate complexing by five-membered ring vic-diols: vapor pressure equilibrium and N.M.R. spectral observations. *Can. J. Chem.* **41**, 2403–2411 (1963).
21. Loomis, W. D. & Durst, R. W. Chemistry and biology of boron. *Biofactors* **3**, 229–239 (1992).
22. Schummer, D., Schomburg, D., Irshik, H., Reichenbach, H. & Höfle, G. Absolute configuration and biosynthesis of tartrolon B, a boron-containing macrodiolide from *Sorangium cellulosum*. *Liebigs Ann. Chemie* **1996**, 965–969 (1996).
23. Otwinowski, Z. & Minor, W. Processing of X-ray diffraction data collected in oscillation mode. *Methods Enzymol.* **276**, 307–326 (1997).
24. Terwilliger, T. C. & Berendzen, J. Automated structure solution for MIR and MAD. *Acta Crystallogr. D* **55**, 849–861 (1999).
25. Collaborative Computational Project Number 4. The CCP4 suite: programs for protein crystallography. *Acta Crystallogr. D* **50**, 760–763 (1994).

26. Jones, T. A., Zou, J.-Y., Cowan, S. W. & Kjeldgaard, M. Improved methods for building protein models in electron density maps and the location of errors in these models. *Acta Crystallogr. A* **47**, 110–119 (1991).
27. Brunger, A. T. *et al.* Crystallography and NMR system (CNS): a new software system for macromolecular structure determination. *Acta Crystallogr. D* **54**, 905–921 (1998).
28. Kraulis, P. MOLSCRIPT: a program to produce both detailed and schematic plots of protein structures. *J. Appl. Crystallogr.* **24**, 924–950 (1991).
29. Esnouf, R. M. An extensively modified version of MolScript that includes greatly enhanced coloring capabilities. *J. Mol. Graph. Model.* **15**, 132–134 (1997).
30. Merritt, E. A. & Bacon, D. J. Raster 3D: photorealistic molecular graphics. *Methods Enzymol.* **277**, 505–524 (1997).
31. O'Neill, M. A., Eberhard, S., Albersheim, P. & Darvill, A. G. Requirement of borate cross-linking of cell wall rhamnogalacturonan II for *Arabidopsis* growth. *Science* **294**, 846–849 (2001).

Acknowledgements

We acknowledge S. Cooper for suggesting that AI-2 could be a cyclic borate diester. We thank R. Carroll, M. Case, S. Miller, K. Xavier and A. Saxena and the staff of the National Synchrotron Light Source beamline X12C for technical assistance, and J. Carey, C. Eckhart, D. Kahne, C. Lee, Y. Shi, K. Shokat, T. Silhavy, and members of the Hughson and Bassler laboratories for discussions. This research was supported by a Deutsche Akademischer Austauschdienst (DAAD) fellowship (S.S.), NSF and the Office of Naval Research (ONR) (B.L.B.), and NIH (F.M.H.).

Correspondence and requests for materials should be addressed to F.M.H. (e-mail: hughson@princeton.edu). Atomic coordinates for the LuxP-AI-2 complex have been deposited in the Protein Data Bank under the accession code 1JX6.

.....
Mutual synergistic folding in recruitment of CBP/p300 by p160 nuclear receptor coactivators

Stephen J. Demarest^{*}, Maria Martinez-Yamout^{*}, John Chung^{*}, Hongwu Chen^{†‡}, Wei Xu[†], H. Jane Dyson^{*}, Ronald M. Evans[†] & Peter E. Wright^{*§}

^{*} Department of Molecular Biology and § The Skaggs Institute for Chemical Biology, The Scripps Research Institute, 10550 North Torrey Pines Road, La Jolla, California 92037, USA

[†] Howard Hughes Medical Institute and The Salk Institute for Biological Studies, La Jolla, California 92037, USA

.....
Nuclear hormone receptors are ligand-activated transcription factors that regulate the expression of genes that are essential for development, reproduction and homeostasis¹. The hormone response is mediated through recruitment of p160 receptor coactivators and the general transcriptional coactivator CBP/p300, which function synergistically to activate transcription². These coactivators exhibit intrinsic histone acetyltransferase activity, function in the remodelling of chromatin, and facilitate the recruitment of RNA polymerase II and the basal transcription machinery³. The activities of the p160 coactivators are dependent on CBP. Both coactivators are essential for proper cell-cycle control, differentiation and apoptosis, and are implicated in cancer and other diseases^{4–7}. To elucidate the molecular basis of assembling the multiprotein activation complex, we undertook a structural and thermodynamic analysis of the interaction domains of CBP and the activator for thyroid hormone and retinoid receptors⁸. Here we show that although the isolated domains are intrinsically disordered, they combine with high affinity to form a cooperatively folded helical heterodimer. Our study uncovers a unique mechanism, called 'synergistic folding', through which p160 coactivators recruit CBP/p300 to allow

[‡] Present address: Department of Biological Chemistry, Cancer Center, University of California, Davis, California 95817, USA.